

1 **MitoChime: A Machine-Learning Pipeline for**
2 **Detecting PCR-Induced Chimeras in**
3 **Mitochondrial Illumina Reads**

4 A Special Project Proposal
5 Presented to
6 the Faculty of the Division of Physical Sciences and Mathematics
7 College of Arts and Sciences
8 University of the Philippines Visayas
9 Miag-ao, Iloilo

10 In Partial Fulfillment
11 of the Requirements for the Degree of
12 Bachelor of Science in Computer Science

13 by

14 Duranne Duran
15 Yvonne Lin
16 Daniella Pailden

17 Adviser
18 Francis D. Dimzon, Ph.D.

19 December 5, 2025

Contents

21	1 Introduction	1
22	1.1 Overview	1
23	1.2 Problem Statement	3
24	1.3 Research Objectives	4
25	1.3.1 General Objective	4
26	1.3.2 Specific Objectives	4
27	1.4 Scope and Limitations of the Research	5
28	1.5 Significance of the Research	6
29	2 Review of Related Literature	7
30	2.1 The Mitochondrial Genome	7
31	2.1.1 Mitochondrial Genome Assembly	8

32	2.2 PCR Amplification and Chimera Formation	9
33	2.3 Existing Traditional Approaches for Chimera Detection	10
34	2.3.1 UCHIME	11
35	2.3.2 UCHIME2	12
36	2.3.3 CATch	13
37	2.3.4 ChimPipe	14
38	2.4 Machine Learning Approaches for Chimera and Sequence Quality	
39	Detection	15
40	2.4.1 Feature-Based Representations of Genomic Sequences . . .	16
41	2.5 Synthesis of Chimera Detection Approaches	18
42	3 Research Methodology	21
43	3.1 Research Activities	21
44	3.1.1 Data Collection	22
45	3.1.2 Bioinformatics Tools Pipeline	26
46	3.1.3 Machine Learning Model Development	29
47	3.1.4 Model Benchmarking, Hyperparameter Optimization, and	
48	Evaluation	30
49	3.1.5 Feature Importance and Interpretation	31

50	3.1.6 Validation and Testing	32
51	3.1.7 Documentation	33
52	3.2 Calendar of Activities	34
53	4 Results and Discussion	35
54	4.1 Descriptive Analysis of Features	35
55	4.1.1 Univariate Distributions	36
56	4.2 Baseline Classification Performance	38
57	4.3 Effect of Hyperparameter Tuning	39
58	4.4 Detailed Evaluation of Representative Models	41
59	4.4.1 Confusion Matrices and Error Patterns	42
60	4.4.2 ROC and Precision–Recall Curves	43

⁶¹ List of Figures

⁶²	3.1 Process Diagram of Special Project	22
⁶³	4.1 Kernel density plots of six key features comparing clean and	
⁶⁴	chimeric reads.	37
⁶⁵	4.2 Test F1 of all baseline classifiers, showing that no single model	
⁶⁶	clearly dominates and several achieve comparable performance. . .	39
⁶⁷	4.3 Comparison of test F1 (left) and ROC–AUC (right) for baseline and	
⁶⁸	tuned models. Hyperparameter tuning yields small but consistent	
⁶⁹	gains, particularly for tree-based ensembles.	41
⁷⁰	4.4 Confusion matrices for the four representative models on the held-	
⁷¹	out test set. All models show more false negatives (chimeric reads	
⁷²	called clean) than false positives.	43
⁷³	4.5 ROC (left) and precision–recall (right) curves for the four represen-	
⁷⁴	tative models on the held-out test set. Tree-based ensembles cluster	
⁷⁵	closely, with logistic regression performing slightly but consistently	
⁷⁶	worse.	44

77 List of Tables

78	2.1 Comparison of Chimera Detection Methods	19
79	3.1 Timetable of Activities	34
80	4.1 Performance of baseline classifiers on the held-out test set.	39
81	4.2 Performance of tuned classifiers on the held-out test set.	40

⁸² **Chapter 1**

⁸³ **Introduction**

⁸⁴ **1.1 Overview**

⁸⁵ The rapid advancement of next-generation sequencing (NGS) technologies has
⁸⁶ transformed genomic research by enabling high-throughput and cost-effective
⁸⁷ DNA analysis (Metzker, 2010). Among current platforms, Illumina sequencing
⁸⁸ remains the most widely adopted, capable of producing millions of short reads
⁸⁹ that can be assembled into reference genomes or analyzed for genetic variation
⁹⁰ (Bentley et al., 2008; Glenn, 2011). Despite its high base-calling accuracy,
⁹¹ Illumina sequencing is prone to artifacts introduced during library preparation,
⁹² particularly polymerase chain reaction (PCR)-induced chimeras, which are ar-
⁹³ tificial hybrid sequences that do not exist in the true genome (Judo, Wedel, &
⁹⁴ Wilson, 1998).

⁹⁵ PCR chimeras form when incomplete extension products from one template

anneal to an unrelated DNA fragment and are extended, creating recombinant reads (Qiu et al., 2001). In mitochondrial genome assembly, such artifacts are especially problematic because the mitochondrial genome is small, circular, and often repetitive (Boore, 1999; Cameron, 2014). Even a small number of chimeric or misjoined reads can reduce assembly contiguity and introduce false junctions during organelle genome reconstruction (Dierckxsens, Mardulyn, & Smits, 2017; Hahn, Bachmann, & Chevreux, 2013; Jin et al., 2020). Existing assembly tools such as GetOrganelle and MITObim assume that input reads are largely free of such artifacts (Hahn et al., 2013; Jin et al., 2020). Consequently, undetected chimeras may produce fragmented assemblies or misidentified organellar boundaries. To ensure accurate reconstruction of mitochondrial genomes, a reliable method for detecting and filtering PCR-induced chimeras before assembly is essential.

This study focuses on mitochondrial sequencing data from the genus *Sardinella*, a group of small pelagic fishes widely distributed in Philippine waters. Among them, *Sardinella lemuru* (Bali sardinella) is one of the country's most abundant and economically important species, providing protein and livelihood to coastal communities (Labrador, Agmata, Palermo, Ravago-Gotanco, & Pante, 2021; Willette, Bognot, Mutia, & Santos, 2011). Accurate mitochondrial assemblies are critical for understanding its population genetics, stock structure, and evolutionary history. However, assembly pipelines often encounter errors or fail to complete due to undetected chimeric reads. To address this gap, this research introduces MitoChime, a machine learning pipeline designed to detect and filter PCR-induced chimeric reads using both alignment-based and sequence-derived statistical features. The tool aims to provide bioinformatics laboratories, partic-

121 ularly the Philippine Genome Center Visayas (PGC Visayas), with an efficient
122 solution for improving mitochondrial genome reconstruction.

123 1.2 Problem Statement

124 While NGS technologies have revolutionized genomic data acquisition, the ac-
125 curacy of mitochondrial genome assembly remains limited by artifacts produced
126 during PCR amplification. These chimeric reads can distort assembly graphs and
127 cause misassemblies, with particularly severe effects in small, circular mitochon-
128 drial genomes (Boore, 1999; Cameron, 2014). Existing assembly pipelines such
129 as GetOrganelle, MITObim, and NOVOPlasty assume that sequencing reads are
130 free of such artifacts (Dierckxsens et al., 2017; Hahn et al., 2013; Jin et al., 2020).
131 At PGC Visayas, several mitochondrial assemblies have failed or yielded incom-
132 plete contigs despite sufficient coverage, suggesting that undetected chimeric reads
133 compromise assembly reliability. Meanwhile, existing chimera detection tools such
134 as UCHIME and VSEARCH were developed primarily for amplicon-based com-
135 munity analysis and rely heavily on reference or taxonomic comparisons (Edgar,
136 Haas, Clemente, Quince, & Knight, 2011; Rognes, Flouri, Nichols, Quince, &
137 Mahé, 2016). These approaches are unsuitable for single-species organellar data,
138 where complete reference genomes are often unavailable. Therefore, there is a
139 pressing need for a reference-independent, data-driven tool capable of detecting
140 and filtering PCR-induced chimeras in mitochondrial sequencing datasets.

¹⁴¹ 1.3 Research Objectives

¹⁴² 1.3.1 General Objective

¹⁴³ This study aims to develop and evaluate a machine learning-based pipeline (Mi-
¹⁴⁴ toChime) that detects PCR-induced chimeric reads in *Sardinella lemuru* mito-
¹⁴⁵ chondrial sequencing data in order to improve the quality and reliability of down-
¹⁴⁶ stream mitochondrial genome assemblies.

¹⁴⁷ 1.3.2 Specific Objectives

¹⁴⁸ Specifically, the study aims to:

- ¹⁴⁹ 1. construct simulated *Sardinella lemuru* Illumina paired-end datasets contain-
¹⁵⁰ ing both clean and PCR-induced chimeric reads,
- ¹⁵¹ 2. extract alignment-based and sequence-based features such as k-mer compo-
¹⁵² sition, junction complexity, and split-alignment counts from both clean and
¹⁵³ chimeric reads,
- ¹⁵⁴ 3. train, validate, and compare supervised machine-learning models for classi-
¹⁵⁵ fying reads as clean or chimeric,
- ¹⁵⁶ 4. determine feature importance and identify indicators of PCR-induced
¹⁵⁷ chimerism,
- ¹⁵⁸ 5. integrate the optimized classifier into a modular and interpretable pipeline
¹⁵⁹ deployable on standard computing environments at PGC Visayas.

160 1.4 Scope and Limitations of the Research

161 This study focuses on detecting PCR-induced chimeric reads in Illumina paired-
162 end mitochondrial sequencing data from *Sardinella lemuru*. The decision to re-
163 strict the taxonomic scope to a single species is based on four considerations:
164 (1) to limit interspecific variation in mitochondrial genome size, GC content, and
165 repetitive regions so that differences in read patterns can be attributed more di-
166 rectly to PCR-induced chimerism; (2) to align the analysis with relevant *S. lemuru*
167 sequencing projects at PGC Visayas; (3) to take advantage of the availability of *S.*
168 *lemuru* mitochondrial assemblies and raw datasets in public repositories such as
169 the National Center for Biotechnology Information (NCBI), which facilitates refer-
170 ence selection and benchmarking; and (4) to develop a tool that directly supports
171 local studies on *S. lemuru* population structure and fisheries management.

172 The study emphasizes `wgsim`-based simulations and selected empirical mito-
173 chondrial datasets from *S. lemuru*. It excludes naturally occurring chimeras, nu-
174 clear mitochondrial pseudogenes (NUMTs), and large-scale assembly rearrange-
175 ments in nuclear genomes. Feature extraction is restricted to low-dimensional
176 alignment and sequence statistics, such as k-mer frequency profiles, GC content,
177 read length, soft and hard clipping metrics, split-alignment counts, and map-
178 ping quality, rather than high-dimensional deep learning embeddings. This de-
179 sign keeps model behaviour interpretable and ensures that the pipeline can be
180 run on standard workstations at PGC Visayas. Testing on long-read platforms
181 (e.g., Nanopore, PacBio) and other taxa is outside the scope of this project; the
182 implemented pipeline is evaluated only on short-read *S. lemuru* datasets.

¹⁸³ **1.5 Significance of the Research**

¹⁸⁴ This research provides both methodological and practical contributions to mi-
¹⁸⁵tochondrial genomics and bioinformatics. First, MitoChime filters PCR-induced
¹⁸⁶ chimeric reads prior to genome assembly, with the goal of improving the con-
¹⁸⁷tiguity and correctness of *Sardinella lemuru* mitochondrial assemblies. Second,
¹⁸⁸ it replaces informal manual curation with a documented workflow, improving au-
¹⁸⁹tomation and reproducibility. Third, the pipeline is designed to run on computing
¹⁹⁰infrastructures commonly available in regional laboratories, enabling routine use
¹⁹¹at facilities such as PGC Visayas. Finally, more reliable mitochondrial assemblies
¹⁹²for *S. lemuru* provide a stronger basis for downstream applications in the field of
¹⁹³fisheries and genomics.

¹⁹⁴ **Chapter 2**

¹⁹⁵ **Review of Related Literature**

¹⁹⁶ This chapter presents an overview of the literature relevant to the study. It
¹⁹⁷ discusses the biological and computational foundations underlying mitochondrial
¹⁹⁸ genome analysis and assembly, as well as existing tools, algorithms, and techniques
¹⁹⁹ related to chimera detection and genome quality assessment. The chapter aims to
²⁰⁰ highlight the strengths, limitations, and research gaps in current approaches that
²⁰¹ motivate the development of the present study.

²⁰² **2.1 The Mitochondrial Genome**

²⁰³ Mitochondrial genome (mtDNA) is a small, typically circular molecule found in
²⁰⁴ most eukaryotes. It encodes essential genes involved in oxidative phosphorylation
²⁰⁵ and energy metabolism. Because of its conserved structure, mtDNA has become
²⁰⁶ a valuable genetic marker for studies in population genetics and phylogenetics
²⁰⁷ (Anderson et al., 1981; Boore, 1999). In animal species, the mitochondrial genome

208 ranges from 15–20 kilobase and contains 13 protein-coding genes, 22 tRNAs, and
209 two rRNAs arranged compactly without introns (Gray, 2012). In comparison to
210 nuclear DNA, the ratio of the number of copies of mtDNA is higher and has
211 simple organization which make it particularly suitable for genome sequencing
212 and assembly studies (Dierckxsens et al., 2017).

213 **2.1.1 Mitochondrial Genome Assembly**

214 Mitochondrial genome assembly refers to the reconstruction of the complete mito-
215 chondrial DNA (mtDNA) sequence from raw or fragmented sequencing reads. It is
216 conducted to obtain high-quality, continuous representations of the mitochondrial
217 genome that can be used for a wide range of analyses, including species identi-
218 fication, phylogenetic reconstruction, evolutionary studies, and investigations of
219 mitochondrial diseases. Because mtDNA evolves rapidly, its assembled sequence
220 provides valuable insights into population structure, lineage divergence, and adap-
221 tive evolution across taxa (Boore, 1999). Compared to nuclear genome assembly,
222 assembling the mitochondrial genome is often considered more straightforward but
223 still encounters technical challenges such as the formation of chimeric reads. Com-
224 monly used tools for mitogenome assembly such as GetOrganelle and MITObim
225 operate under the assumption of organelle genome circularity, and are vulnerable
226 when chimeric reads disrupt this circular structure, resulting in assembly errors
227 (Hahn et al., 2013; Jin et al., 2020).

228 2.2 PCR Amplification and Chimera Formation

229 PCR plays an important role in NGS library preparation, as it amplifies target
230 DNA fragments for downstream analysis. However as previously mentioned, the
231 amplification process can also introduce chimeric reads which compromises the
232 quality of the input reads supplied to sequencing or assembly workflows. Chimeras
233 typically arise when incomplete extension occurs during a PCR cycle. This causes
234 the DNA polymerase to switch from one template to another and generate hy-
235 brid recombinant molecules (Judo et al., 1998). Artificial chimeras are produced
236 through such amplification errors, whereas biological chimeras occur naturally
237 through genomic rearrangements or transcriptional events.

238 In the context of amplicon-based sequencing, the presence of chimeras can in-
239 flate estimates of genetic or microbial diversity and may cause misassemblies dur-
240 ing genome reconstruction. Qin et al. (2023) has reported that chimeric sequences
241 may account for more than 10% of raw reads in amplicon datasets. This artifact
242 tends to be most prominent among rare operational taxonomic units (OTUs) or
243 singletons, which are sometimes misinterpreted as novel diversity, further caus-
244 ing the complication of microbial diversity analyses (Gonzalez, Zimmermann, &
245 Saiz-Jimenez, 2004). As such, determining and minimizing PCR-induced chimera
246 formation is vital for improving the quality of mitochondrial genome assemblies,
247 and ensuring the reliability of amplicon sequencing data.

248 2.3 Existing Traditional Approaches for Chimera

249 Detection

250 Several computational tools have been developed to identify chimeric sequences in
251 NGS datasets. These tools generally fall into two categories: reference-based and
252 de novo approaches. Reference-based chimera detection, also known as database-
253 dependent detection, is one of the earliest and most widely used computational
254 strategies for identifying chimeric sequences in amplicon-based community studies.
255 These methods rely on the comparison of each query sequence against a curated,
256 high-quality database of known, non-chimeric reference sequences (Edgar et al.,
257 2011).

258 On the other hand, the de novo chimera detection, also referred to as reference-
259 free detection, represents an alternative computational paradigm that identifies
260 chimeric sequences without reliance on external reference databases. This method
261 infer chimeras based on internal relationships among the sequences present within
262 the dataset itself, making it particularly advantageous in studies of under explored
263 or taxonomically diverse communities where comprehensive reference databases
264 are unavailable or incomplete (Edgar, 2016; Edgar et al., 2011). The underlying
265 assumption on this method is that during PCR, true biological sequences are
266 generally more abundant as they are amplified early and dominate the read pool,
267 whereas chimeric sequences appear later and are generally less abundant. The
268 de novo approach leverage this abundance hierarchy, treating the most abundant
269 sequences as supposed parents and testing whether less abundant sequences can
270 be reconstructed as mosaics of these templates. Compositional and structural
271 similarity are also evaluated to check whether different regions of a candidate

272 sequence correspond to distinct high-abundance sequences.

273 In practice, many modern bioinformatics pipelines combine both paradigms
274 sequentially: an initial de novo step identifies dataset-specific chimeras, followed
275 by a reference-based pass that removes remaining artifacts relative to established
276 databases (Edgar, 2016). These two methods of detection form the foundation of
277 tools such as UCHIME and later UCHIME2.

278 2.3.1 UCHIME

279 UCHIME is one of the most widely used computational tools for detecting chimeric
280 sequences in amplicon sequencing data, as it serves as a critical quality control
281 step to prevent the misinterpretation of PCR artifacts as novel biological diversity.
282 The algorithm operates by searching for a model (M) where a query (Q) sequence
283 can be perfectly explained as a combination of two parent sequences, denoted as
284 A and B (Edgar et al., 2011).

285 In reference mode, UCHIME divides the query into four chunks and maps
286 them to a trusted chimeric-free database to identify candidate parents. It then
287 constructs a three-way alignment to calculate a score based on “votes.” A “Yes”
288 vote indicates the query aligns with parent A in one region and parent B in an-
289 other, while a “No” vote penalizes the score if the query diverges from the expected
290 chimeric model. In de novo mode, the algorithm operationalizes the abundance
291 skew principle described in Section 2.3. Instead of using an external database,
292 UCHIME dynamically treats the sample’s own high-abundance sequences as a
293 reference database, testing if lower-abundance sequences can be reconstructed as

294 mosaics of these internal ancestors (Edgar et al., 2011).

295 Despite its high sensitivity, UCHIME has inherent limitations rooted in
296 sequence divergence and database quality. The algorithm struggles to detect
297 chimeras formed from parents that are very closely related, specifically when the
298 sequence divergence between parents is less than roughly 0.8%, as the signal-to-
299 noise ratio becomes too low to distinguish a crossover event from sequencing error
300 (Edgar et al., 2011). Furthermore, in reference mode, the accuracy is strictly
301 bound by the completeness of the database; if true parents are absent, the tool
302 may fail to identify the chimera or produce false positives. Similarly, the de novo
303 mode relies on the assumption that parents are present and sufficiently more
304 abundant in the sample, which may not hold true in unevenly amplified samples
305 or complex communities.

306 2.3.2 UCHIME2

307 Building upon the original algorithm, UCHIME2 was developed to address the
308 nuances of high-resolution amplicon sequencing. A key contribution of the
309 UCHIME2 study was the critical re-evaluation of chimera detection benchmarks.
310 In the UCHIME2 paper (Edgar, 2016) and the UCHIME in practice website
311 (Edgar, n.d), the author has noted that the accuracy results reported in the
312 original UCHIME paper were “highly over-optimistic” because they relied on
313 unrealistic benchmark designs where parent sequences were assumed to be 100%
314 known and present. UCHIME2 introduced more rigorous testing (the CHSIMA
315 benchmark), revealing that “fake models,” where a valid biological sequence
316 perfectly mimics a chimera of two other valid sequences, are far more common

317 than previously assumed. This discovery suggests that error-free detection is
318 impossible in principle (Edgar, 2016). Another notable improvement is the in-
319 troduction of multiple application-specific modes that allow users to tailor the
320 algorithm’s performance to the characteristics of their datasets. The following
321 parameter presets: denoised, balanced, sensitive, specific, and high-confidence,
322 enable researchers to optimize the balance between sensitivity and specificity
323 according to the goals of their analysis.

324 However despite these advancements, the practical application of UCHIME2
325 requires caution. The author explicitly advises against using UCHIME2 as
326 a stand-alone tool in standard OTU clustering or denoising pipelines. Using
327 UCHIME2 as an independent filtering step in these workflows is discouraged, as
328 it often results in significantly higher error rates, increasing both false positives
329 (discarding valid sequences) and false negatives (retaining chimeras) (Edgar,
330 2016).

331 2.3.3 CATch

332 As previously mentioned, UCHIME (Edgar et al., 2011) relied on alignment-based
333 sequences in amplicon data. However, researchers soon observed that different al-
334 gorithms often produced inconsistent predictions. A sequence might be identified
335 as chimeric by one tool but classified as non-chimeric by another, resulting in
336 unreliable filtering outcomes across studies.

337 To address these inconsistencies, Mysara, Saeys, Leys, Raes, and Monsieurs
338 (2015) developed the Classifier for Amplicon Tool Chimeras (CATCh), which rep-

339 resents the first ensemble machine learning system designed for chimera detection
340 in 16S rRNA amplicon sequencing. Rather than depending on a single detec-
341 tion strategy, CATCh integrates the outputs of several established tools, includ-
342 ing UCHIME, ChimeraSlayer, DECIPHER, Pintail, and Perseus. The individual
343 scores and binary decisions generated by these tools are used as input features for
344 a supervised learning model. The algorithm employs a Support Vector Machine
345 (SVM) with a Pearson VII Universal Kernel (PUK) to determine optimal weight-
346 ings among the input features and to assign each sequence a probability of being
347 chimeric.

348 Benchmarking in both reference-based and de novo modes demonstrated signif-
349 icant performance improvements. CATCh achieved sensitivities of approximately
350 85 percent in reference-based mode and 92 percent in de novo mode, with corre-
351 sponding specificities of approximately 96 percent and 95 percent. These results
352 indicate that CATCh detected 7 to 12 percent more chimeras than any individual
353 algorithm while maintaining high precision.

354 **2.3.4 ChimPipe**

355 Among the available tools for chimera detection, ChimPipe is a pipeline developed
356 to identify chimeric sequences such as biological chimeras. It uses both discordant
357 paired-end reads and split-read alignments to improve the accuracy and sensitivity
358 of detecting biological chimeras (Rodriguez-Martin et al., 2017). By combining
359 these two sources of information, ChimPipe achieves better precision than meth-
360 ods that depend on a single type of indicator.

361 The pipeline works with many eukaryotic species that have available genome
362 and annotation data (Rodriguez-Martin et al., 2017). It can also predict multiple
363 isoforms for each gene pair and identify breakpoint coordinates that are useful
364 for reconstructing and verifying chimeric transcripts. Tests using both simulated
365 and real datasets have shown that ChimPipe maintains high accuracy and reliable
366 performance.

367 ChimPipe lets users adjust parameters to fit different sequencing protocols or
368 organism characteristics. Experimental results have confirmed that many chimeric
369 transcripts detected by the tool correspond to functional fusion proteins, demon-
370 strating its utility for understanding chimera biology and its potential applications
371 in disease research (Rodriguez-Martin et al., 2017).

372 **2.4 Machine Learning Approaches for Chimera 373 and Sequence Quality Detection**

374 Traditional chimera detection tools rely primarily on heuristic or alignment-based
375 rules. Recent advances in machine learning (ML) have demonstrated that models
376 trained on sequence-derived features can effectively capture compositional and
377 structural patterns in biological sequences. Although most existing ML systems
378 such as those used for antibiotic resistance prediction, taxonomic classification,
379 or viral identification are not specifically designed for chimera detection, they
380 highlight how data-driven models can outperform similarity-based heuristics by
381 learning intrinsic sequence signatures. In principle, ML frameworks can integrate
382 indicators such as k-mer frequencies, GC-content variation and split-alignment

383 metrics to identify subtle anomalies that may indicate a chimeric origin (Arango
384 et al., 2018; Liang, Bible, Liu, Zou, & Wei, 2020; Ren et al., 2020).

385 **2.4.1 Feature-Based Representations of Genomic Se-**
386 **quences**

387 In genomic analysis, feature extraction converts DNA sequences into numerical
388 representations suitable for ML algorithms. A common approach is k-mer fre-
389 quency analysis, where normalized k-mer counts form the feature vector (Vervier,
390 Mahé, Tournoud, Veyrieras, & Vert, 2015). These features effectively capture lo-
391 cal compositional patterns that often differ between authentic and chimeric reads.

392 In particular, deviations in k-mer profiles between adjacent read segments can
393 serve as a compositional signature of template-switching events. Additional de-
394 scriptors such as GC content and sequence entropy can further distinguish se-
395 quence types; in metagenomic classification and virus detection, k-mer-based fea-
396 tures have shown strong performance and robustness to noise (Ren et al., 2020;
397 Vervier et al., 2015). For chimera detection specifically, abrupt shifts in GC or k-
398 mer composition along a read can indicate junctions between parental fragments.
399 Windowed feature extraction enables models to capture these discontinuities that
400 rule-based algorithms may overlook.

401 Machine learning models can also leverage alignment-derived features such as
402 the frequency of split alignments, variation in mapping quality, and local cover-
403 age irregularities. Split reads and discordant read pairs are classical indicators
404 of genomic junctions and have been formalized in probabilistic frameworks for
405 structural-variant discovery that integrate multiple evidence types (Layer, Hall, &

406 Quinlan, 2014). Similarly, long-read tools such as Sniffles employ split-alignment
407 and coverage anomalies to accurately localize breakpoints (Sedlazeck et al., 2018).
408 Modern aligners such as Minimap2 (Li, 2018) output supplementary (SA tags) and
409 secondary alignments as well as chaining and alignment-score statistics that can
410 be summarized into quantitative predictors for machine-learning models. These
411 alignment-signal features are particularly relevant to PCR-induced mitochondrial
412 chimeras, where template-switching events produce reads partially matching dis-
413 tinct regions of the same or related genomes. Integrating such cues within a
414 supervised-learning framework enables artifact detection even in datasets lacking
415 complete or perfectly assembled references.

416 A further biologically grounded descriptor is the length of microhomology at
417 putative junctions. Microhomology refers to short, shared sequences, often in the
418 range of a few to tens of base pairs that are near breakpoints where template-
419 switching events typically happen. Studies of double strand break repair and
420 structural variation have demonstrated that the length of microhomology corre-
421 lates with the likelihood of microhomology-mediated end joining (MMEJ) or fork-
422 stalled template-switching pathways (Sfeir & Symington, 2015). In the context of
423 PCR-induced chimeras, template switching during amplification often leaves short
424 identical sequences at the junction of two concatenated fragments. Quantifying
425 the longest exact suffix–prefix overlap at each candidate breakpoint thus provides
426 a mechanistic signature of chimerism and complements both compositional (k-
427 mer) and alignment (SA count) features.

428 2.5 Synthesis of Chimera Detection Approaches

429 To provide an integrated overview of the literature discussed in this chapter, Ta-
430 ble 2.1 summarizes the major chimera detection studies, their methodological
431 approaches, and their known limitations.

Table 2.1: Comparison of Chimera Detection Methods

Methods	Approach	Limitations
Reference-based Chimera Detection	Compares query sequences against curated, non-chimeric reference databases; identifies mosaic sequences by evaluating similarity to known templates.	Depends heavily on completeness and quality of reference databases; often fails when novel taxa or missing parent sequences are present; reduced accuracy for low-divergence chimeras.
De novo Chimera Detection	Identifies chimeras using only internal dataset relationships; relies on abundance patterns and compositional similarity; reconstructs sequences as mosaics of high-abundance parents.	Assumes true sequences are more abundant—fails when amplification bias distorts abundance; struggles with evenly abundant parental sequences; can misclassify highly similar true variants.
UCHIME	Alignment-based chimera detection; segments query sequence, identifies parent candidates, performs 3-way alignment, and computes chimera scores; supports both reference-based and de novo modes.	Accuracy inflated in original benchmarks; suffers under incomplete databases; poor performance on low-divergence chimeras; sensitive to sequencing errors; misclassifies when parents are missing.
UCHIME2	Improved initial UCHIME benchmarking; offers multiple sensitivity/specificity modes; more robust with incomplete references; higher sensitivity.	Cannot achieve perfect accuracy due to “perfect fake models”; genuine variants may be indistinguishable from artificial recombinants; theoretical detection limit remains.
CATCh	First ML ensemble tool for 16S chimera detection; integrates outputs of UCHIME, ChimeraSlayer, DECIPHER, Pintail, Perseus via SVM classifier; significantly improves sensitivity and specificity.	Depends on performance of underlying tools; ML model limited to features they output; ensemble can still misclassify in datasets with extreme novelty or low coverage.
ChimPipe	Pipeline for detecting fusion genes and transcript-derived chimeras in RNA-seq; uses discordant paired-end reads and split-alignments; predicts isoforms and breakpoint coordinates.	Designed for RNA-seq, not amplicons; needs high-quality genome and annotation; computationally heavier; limited to organisms with reference genomes.

432 Across existing studies, no single approach reliably detects all forms of chimeric
433 sequences, particularly those generated by PCR-induced template switching in
434 mitochondrial genomes. Reference-based tools perform poorly when parental se-
435 quences are absent; de novo methods rely strongly on abundance assumptions;
436 alignment-based systems show reduced sensitivity to low-divergence chimeras; and
437 ensemble methods inherit the limitations of their component algorithms. RNA-
438 seq-oriented pipelines likewise do not generalize well to organelle data. Although
439 machine learning approaches offer promising feature-based detection, they are
440 rarely applied to mitochondrial genomes and are not trained specifically on PCR-
441 induced organelle chimeras. These limitations indicate a clear research gap: the
442 need for a specialized, feature-driven classifier tailored to mitochondrial PCR-
443 induced chimeras that integrates k-mer composition, split-alignment signals, and
444 micro-homology features to achieve more accurate detection than current heuristic
445 or alignment-based tools.

⁴⁴⁶ Chapter 3

⁴⁴⁷ Research Methodology

⁴⁴⁸ This chapter outlines the steps involved in completing the study, including data
⁴⁴⁹ gathering, generating simulated mitochondrial Illumina reads, preprocessing and
⁴⁵⁰ indexing the data, developing a bioinformatics pipeline to extract key features,
⁴⁵¹ applying machine learning algorithms for chimera detection, and validating and
⁴⁵² comparing model performance.

⁴⁵³ 3.1 Research Activities

⁴⁵⁴ As illustrated in Figure 3.1, this study carried out a sequence of procedures to
⁴⁵⁵ detect PCR-induced chimeric reads in mitochondrial genomes. The process began
⁴⁵⁶ with collecting a mitochondrial reference sequence of *Sardinella lemuru* from the
⁴⁵⁷ National Center for Biotechnology Information (NCBI) database, which was used
⁴⁵⁸ as a reference for generating simulated clean and chimeric reads. These reads
⁴⁵⁹ were subsequently indexed and mapped. The resulting collections then passed

460 through a bioinformatics pipeline that extracted k-mer profiles, supplementary
461 alignment (SA) features, and microhomology information to prepare the data for
462 model construction. The machine learning model was trained using the processed
463 input, and its precision and accuracy were assessed. It underwent tuning until it
464 reached the desired performance threshold, after which it proceeded to validation
465 and will undergo testing.

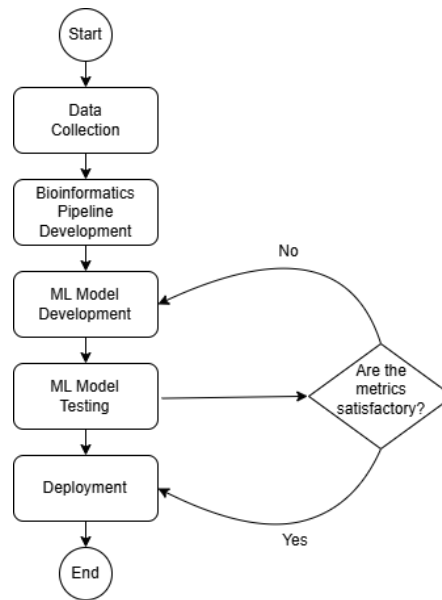


Figure 3.1: Process Diagram of Special Project

466 3.1.1 Data Collection

467 The mitochondrial genome reference sequence of *S. lemuru* was obtained from the
468 NCBI database (accession number NC_039553.1) in FASTA format. This sequence
469 served as the basis for generating simulated reads for model development.

470 This step was scheduled to begin in the first week of November 2025 and
471 expected to be completed by the end of that week, with a total duration of ap-

472 proximately one (1) week.

473 Data Preprocessing

474 To reduce manual repetition, all steps in the simulation and preprocessing pipeline
475 were executed using a custom script in Python (Version 3.11). The script runs
476 each stage, including read simulation, reference indexing, mapping, and alignment
477 processing, in a fixed sequence.

478 Sequencing data were simulated from the NCBI reference genome using `wgsim`
479 (Version 1.13). First, a total of 10,000 paired-end fragments were simulated,
480 producing 20,000 reads (10,000 forward and 10,000 reverse) from the the original
481 reference (`original_reference.fasta`) and and designated as clean reads using
482 the command:

```
483 wgsim -1 150 -2 150 -r 0 -R 0 -X 0 -e 0.001 -N 10000 \  
484     original_reference.fasta ref1.fastq ref2.fastq
```

485 The command parameters are as follows:

- 486 • `-1` and `-2`: read lengths of 150 base pairs for each paired-end read.
- 487 • `-r`, `-R`, `-X`: mutation rate, fraction of indels, and indel extension probability,
488 all set to a default value of 0.
- 489 • `-e`: base error rate, set to 0.001 to simulate realistic sequencing errors.
- 490 • `-N`: number of read pairs, set to 10,000.

491 Chimeric sequences were then generated from the same NCBI reference using a
492 separate Python script. Two non-adjacent segments were randomly selected such
493 that their midpoint distances fell within specified minimum and maximum thresh-
494 olds. The script attempts to retain microhomology, or short identical sequences
495 at segment junctions, to mimic PCR-induced template switching. The resulting
496 chimeras were written to `chimera_reference.fasta`, with headers recording seg-
497 ment positions and microhomology length. The `chimera_reference.fasta` was
498 processed with `wgsim` to simulate 10,000 paired-end fragments, generating 20,000
499 chimeric reads (10,000 forward reads in `chimeric1.fastq` and 10,000 reverse reads
500 in `chimeric2.fastq`) using the command format.

501 Next, a `minimap2` index of the reference genome was created using:

```
502 minimap2 -d ref.mmi original_reference.fasta
```

503 Minimap2 (Version 2.28) is a tool used to map reads to a reference genome.
504 The index `ref.mmi` of the original reference sequence is required by `minimap2` for
505 efficient read mapping. Mapping allows extraction of alignment features from each
506 read, which were used as input for the machine learning model. The simulated
507 clean and chimeric reads were then mapped to the reference index as follows:

```
508 minimap2 -ax sr -t 8 ref.mmi ref1.fastq ref2.fastq > clean.sam
```

```
509 minimap2 -ax sr -t 8 ref.mmi \  
510 chimeric1.fastq chimeric2.fastq > chimeric.sam
```

511 Here, `-ax sr` specifies short-read alignment mode, and `-t 8` uses 8 CPU

512 threads. The resulting clean and chimeric SAM files contain the alignment posi-
513 tions of each read relative to the original reference genome.

514 The SAM files were then converted to BAM format, sorted, and indexed using

515 `samtools` (Version 1.20):

```
516 samtools view -bS clean.sam -o clean.bam  
517 samtools view -bS chimeric.sam -o chimeric.bam  
518  
519 samtools sort clean.bam -o clean.sorted.bam  
520 samtools index clean.sorted.bam  
521  
522 samtools sort chimeric.bam -o chimeric.sorted.bam  
523 samtools index chimeric.sorted.bam
```

524 BAM files are the compressed binary version of SAM files, which enables faster
525 processing and reduced storage. Sorting arranges reads by genomic coordinates,
526 and indexing allows detection of SA as a feature for the machine learning model.

527 The total number of simulated reads was expected to be 40,000. The final col-
528 lection of reads contained 19,984 clean reads and 20,000 chimeric reads (39,984 en-
529 tries in total), providing a roughly balanced distribution between the two classes.
530 After alignment with `minimap2`, only 19,984 clean reads remained because un-
531 mapped reads were not included in the BAM file. Some sequences failed to align
532 due to the 5% error rate defined during `wgsim` simulation, which produced mis-
533 matches that caused certain reads to fall below the aligner's matching threshold.

534 This whole process is scheduled to start in the second week of November 2025

535 and is expected to be completed by the last week of November 2025, with a total
536 duration of approximately three (3) weeks.

537 **3.1.2 Bioinformatics Tools Pipeline**

538 A bioinformatics pipeline will be developed and implemented to extract the neces-
539 sary analytical features. This pipeline will function as a reproducible and modular
540 workflow that accepts FASTQ and BAM/SAM file inputs, processes them using
541 tools such as `samtools` and `jellyfish` (Version 2.3.1), and produces tabular fea-
542 ture matrices (TSV) for downstream machine learning. To ensure correctness
543 and adherence to best practices, bioinformatics experts at the PGC Visayas will
544 be consulted to validate the pipeline design, feature extraction logic, and overall
545 data integrity. This stage of the study is scheduled to begin in the first week of
546 January 2026 and conclude by the last week of February 2026, with an estimated
547 total duration of approximately two (2) months.

548 The bioinformatics pipeline focuses on three principal features from the simu-
549 lated and aligned sequencing data: (1) supplementary alignment flag (SA count),
550 (2) k-mer composition difference between read segments, and (3) microhomology
551 length at potential junctions. Each of these features captures a distinct biological
552 or computational signature associated with PCR-induced chimeras.

553 **Supplementary Alignment Flag**

554 Supplementary alignment information will be assessed using the mapped and
555 sorted BAM files (`clean.sorted.bam` and `chimeric.sorted.bam`) generated

556 from the data preprocessing stage. Alignment summaries will be checked using
557 `samtools flagstat` to obtain preliminary quality-control statistics, including
558 counts of primary, secondary, and supplementary (SA) alignments.

559 Both BAM files will be converted to SAM format for detailed inspection of
560 reads in each file:

```
561 samtools view -h clean.sorted.bam -o clean.sorted.sam  
562 samtools view -h chimeric.sorted.bam -o chimeric.sorted.sam
```

563 The SAM output will be checked for reads containing the SA:Z flag, as it
564 denotes supplementary alignments. Reads exhibiting these or substantial soft-
565 clipped regions will be considered strong candidates for chimeric artifacts. A
566 custom Python script would be created to extract the alignment-derived features
567 and relevant metadata including mapping quality, SAM flag information, CIGAR-
568 based clipping, and alignment coordinates. These extracted attributes would then
569 be organized and compiled into a TSV (`.tsv`) file.

570 K-mer Composition Difference

571 Chimeric reads often comprise fragments from distinct genomic regions, resulting
572 in a compositional discontinuity between segments. Comparing k-mer frequency
573 profiles between the left and right halves of a read allows detection of such abrupt
574 compositional shifts, independent of alignment information. This will be obtained
575 using Jellyfish, a fast k-mer counting software. For each read, the sequence will
576 be divided into two segments, either at the midpoint or at empirically determined
577 breakpoints inferred from supplementary alignment data, to generate left and right

578 sequence segments. Jellyfish will then compute k-mer frequency profiles (with $k =$
579 5 or 6) for each segment. The resulting k-mer frequency vectors will be normalized
580 and compared using distance metrics such as cosine similarity or Jensen–Shannon
581 divergence to quantify compositional disparity between the two halves of the same
582 read. The resulting difference scores will be stored in a structured TSV file.

583 Microhomology Length

584 The microhomology length was computed as part of the bioinformatics pipeline.
585 For each aligned read in the BAM files, the script first inferred a breakpoint
586 using the function `infer_breakpoint`, which represents a junction between two
587 segments. Breakpoints were determined primarily from soft-clipping patterns.
588 If no soft clips were present, SA tags were used to identify potential alignment
589 discontinuities.

590 Once a breakpoint was established, the script scanned a ± 40 base pair window
591 surrounding the breakpoint and used the function `longest_suffix_prefix_overlap`
592 to identify the longest exact suffix-prefix overlap between the left and right read
593 segments. This overlap, which represents consecutive bases shared at the junc-
594 tion, was recorded as the microhomology length. Additionally, the GC content
595 of the overlapping sequence was calculated using the function `gc_content`, which
596 counts guanine (G) and cytosine (C) bases within the detected microhomology
597 and divides by the total length, yielding a proportion between 0 and 1.

598 Short microhomologies, typically 3-20 base pairs in length, are recognized sig-
599 natures of PCR-induced template switching and can promote template recombi-
600 nation (Peccoud et al., 2018). Each read was annotated after capturing both the

601 length and GC content of microhomology.

602 3.1.3 Machine Learning Model Development

603 After feature extraction, the per-read feature matrices for clean and chimeric
604 reads were merged into a single dataset. Each row corresponded to one paired-
605 end read, and columns encoded alignment-structure features (e.g., supplementary
606 alignment count and spacing between segments), CIGAR-derived soft-clipping
607 statistics (e.g., left and right soft-clipped length, total clipped bases), k-mer com-
608 position discontinuity between read segments, and microhomology descriptors
609 near candidate junctions. The resulting feature set was restricted to quantities
610 that can be computed from standard BAM/FASTQ files in typical mitochondrial
611 sequencing workflows.

612 The labelled dataset was randomly partitioned into training (80%) and test
613 (20%) subsets using stratified sampling to preserve the 1:1 ratio of clean to
614 chimeric reads. Model development and evaluation were implemented in Python
615 (Version 3.11) using the `scikit-learn`, `xgboost`, `lightgbm`, and `catboost` li-
616 braries. A broad panel of classification algorithms was then benchmarked on the
617 training data to obtain a fair comparison of different model families under identical
618 feature conditions. The panel included: a trivial dummy classifier, L2-regularized
619 logistic regression, a calibrated linear support vector machine (SVM), k -nearest
620 neighbours, Gaussian Naïve Bayes, decision-tree ensembles (Random Forest, Ex-
621 tremely Randomized Trees, and Bagging with decision trees), gradient boosting
622 methods (Gradient Boosting, XGBoost, LightGBM, and CatBoost), and a shallow
623 multilayer perceptron (MLP).

624 For each model, five-fold stratified cross-validation was performed on the train-
625 ing set. In every fold, four-fifths of the data were used for fitting and the remaining
626 one-fifth for validation. Mean cross-validation accuracy, precision, recall, F1-score
627 for the chimeric class, and area under the receiver operating characteristic curve
628 (ROC–AUC) were computed to summarize performance and rank candidate meth-
629 ods. This baseline screen allowed comparison of linear, probabilistic, neural, and
630 ensemble-based approaches and identified tree-based ensemble and boosting mod-
631 els as consistently strong performers relative to simpler baselines.

632 **3.1.4 Model Benchmarking, Hyperparameter Optimiza-
633 tion, and Evaluation**

634 Model selection and refinement proceeded in two stages. First, the cross-validation
635 results from the broad panel were used to identify a subset of competitive mod-
636 els for more detailed optimization. Specifically, ten model families were carried
637 forward: L2-regularized logistic regression, calibrated linear SVM, Random For-
638 est, ExtraTrees, Gradient Boosting, XGBoost, LightGBM, CatBoost, Bagging
639 with decision trees, and a shallow MLP. This subset spans both linear and non-
640 linear decision boundaries, but emphasizes ensemble and boosting methods, which
641 showed superior F1 and ROC–AUC in the initial benchmark.

642 Second, hyperparameter optimization was conducted for each of the ten se-
643 lected models using randomized search with five-fold stratified cross-validation
644 (`RandomizedSearchCV`). For tree-based ensembles, the search space included the
645 number of trees, maximum depth, minimum samples per split and leaf, and the
646 fraction of features considered at each split. For boosting methods, key hyper-

647 parameters such as the number of boosting iterations, learning rate, tree depth,
648 subsampling rate, and column subsampling rate were tuned. For the MLP, the
649 number and size of hidden layers, learning rate, and L_2 regularization strength
650 were varied. In all cases, the primary optimisation criterion was the F1-score of
651 the chimeric class, averaged across folds.

652 For each model family, the hyperparameter configuration with the highest
653 mean cross-validation F1-score was selected as the best-tuned estimator. These
654 tuned models were then refitted on the full training set and evaluated once on the
655 held-out test set to obtain unbiased estimates of performance. Test-set metrics in-
656 cluded accuracy, precision, recall, F1-score for the chimeric class, and ROC–AUC.
657 Confusion matrices and ROC curves were generated for the top-performing mod-
658 els to characterise common error modes, such as false negatives (missed chimeric
659 reads) and false positives (clean reads incorrectly labelled as chimeric). The final
660 model or small set of models for downstream interpretation was chosen based on
661 a combination of test-set F1-score, ROC–AUC, and practical considerations such
662 as model complexity and ease of deployment within a bioinformatics pipeline.

663 3.1.5 Feature Importance and Interpretation

664 To relate model decisions to biologically meaningful signals, feature-importance
665 analyses were performed on the best-performing tree-based models. Two comple-
666 mentary approaches were used. First, built-in importance measures from ensemble
667 methods (e.g., split-based importances in Random Forest and Gradient Boosting)
668 were examined to obtain an initial ranking of features based on their contribution
669 to reducing impurity. Second, model-agnostic permutation importance was com-

670 puted on the test set by repeatedly permuting each feature column while keeping
671 all others fixed and measuring the resulting decrease in F1-score. Features whose
672 permutation led to a larger performance drop were interpreted as more influential
673 for chimera detection.

674 For interpretability, individual features were grouped into four conceptual
675 families: (i) supplementary alignment and alignment-structure features (e.g., SA
676 count, spacing between alignment segments, strand consistency), (ii) CIGAR-
677 derived soft-clipping features (e.g., left and right soft-clipped length, total clipped
678 bases), (iii) k-mer composition discontinuity features (e.g., cosine distance and
679 Jensen–Shannon divergence between k-mer profiles of read segments), and (iv) mi-
680 crohomology descriptors (e.g., microhomology length and local GC content around
681 putative breakpoints). Aggregating permutation importance scores within each
682 family allowed assessment of which biological signatures contributed most strongly
683 to the classifier’s performance. This analysis provided a basis for interpreting the
684 trained models in terms of known mechanisms of PCR-induced template switching
685 and for identifying which alignment- and sequence-derived cues are most informa-
686 tive for distinguishing chimeric from clean mitochondrial reads.

687 3.1.6 Validation and Testing

688 Validation will involve both internal and external evaluations. Internal valida-
689 tion was achieved through five-fold cross-validation on the training data to verify
690 model generalization and reduce variance due to random sampling. External vali-
691 dation will be achieved through testing on the 20% hold-out dataset derived from
692 the simulated reads, which will be an unbiased benchmark to evaluate how well

693 the trained models generalized to unseen data. All feature extraction and pre-
694 processing steps were performed using the same bioinformatics pipeline to ensure
695 consistency and comparability across validation stages.

696 Comparative evaluation was performed across all candidate algorithms, in-
697 cluding a trivial dummy classifier, L2-regularized logistic regression, a calibrated
698 linear SVM, k-nearest neighbours, Gaussian Naïve Bayes, decision-tree ensembles,
699 gradient boosting methods, and a shallow MLP. This evaluation determined which
700 models demonstrated the highest predictive performance and computational effi-
701 ciency under identical data conditions. Their metrics were compared to identify
702 which algorithms were most suitable for further refinement.

703 3.1.7 Documentation

704 Comprehensive documentation was maintained throughout the study to ensure
705 transparency and reproducibility. All stages of the research, including data gath-
706 ering, preprocessing, feature extraction, model training, and validation, were sys-
707 tematically recorded in a `.README` file in the GitHub repository. For each ana-
708 lytical step, the corresponding parameters, software versions, and command line
709 scripts were documented to enable exact replication of results.

710 The repository structure followed standard research data management prac-
711 tices, with clear directories for datasets and scripts. Computational environments
712 were standardized using Conda, with an environment file (`environment.arm.yml`)
713 specifying dependencies and package versions to maintain consistency across sys-
714 tems.

₇₁₅ For manuscript preparation and supplementary materials, Overleaf (L^AT_EX)
₇₁₆ was used to produce publication-quality formatting and consistent referencing. f

₇₁₇ 3.2 Calendar of Activities

₇₁₈ Table 3.1 presents the project timeline in the form of a Gantt chart, where each
₇₁₉ bullet point corresponds to approximately one week of planned activity.

Table 3.1: Timetable of Activities

Activities (2025)	Nov	Dec	Jan	Feb	Mar	Apr	May
Data Collection and Simulation	• • •						
Bioinformatics Tools Pipeline			• • •	• • •			
Machine Learning Development			••	• • •	• • •	••	
Testing and Validation						••	• • •
Documentation	• • •	• • •	• • •	• • •	• • •	• • •	• • •

720 Chapter 4

721 Results and Discussion

722 4.1 Descriptive Analysis of Features

723 This chapter presents the performance of the proposed feature set and machine-
724 learning models for detecting PCR-induced chimeric reads in simulated mitochon-
725 drial Illumina data. We first describe the behaviour of the main features, then
726 compare baseline classifiers, assess the effect of hyperparameter tuning, and fi-
727 nally analyse feature importance in terms of individual variables and biologically
728 motivated feature families.

729 The final dataset contained 31 986 reads for training and 7 997 reads for testing,
730 with classes balanced (approximately 4 000 clean and 4 000 chimeric reads in the
731 test split).

732 4.1.1 Univariate Distributions

733 The kernel density plots in Figures 4.1a–4.1f collectively show that alignment-
734 based features provide the strongest separation between clean and chimeric reads.
735 The distribution of `sa_count` (Figure 4.1a) is distinctly bimodal, with clean reads
736 concentrated near zero and chimeric reads peaking around one, reflecting the
737 frequent presence of supplementary alignments in chimeras. A similar pattern of
738 clear separation is observed in `softclip_left` and `softclip_right` (Figures 4.1c
739 and 4.1d), where clean reads cluster tightly at zero while chimeric reads display
740 broad, long-tailed distributions, consistent with extensive soft clipping when
741 a read spans multiple genomic locations. In contrast, `microhomology_length`
742 (Figure 4.1b) shows substantial overlap between classes, with both distribu-
743 tions sharply concentrated near zero and exhibiting smaller secondary peaks
744 at short integer lengths, indicating limited discriminative value under the sim-
745 ulated conditions. Finally, the k-mer-based features `kmer_js_divergence` and
746 `kmer_cosine_diff` (Figures 4.1e and 4.1f) exhibit highly overlapping, multimodal
747 distributions with both classes peaking near 1.0; although chimeric reads appear
748 slightly less concentrated at the highest similarity values, the separation is weak
749 overall.

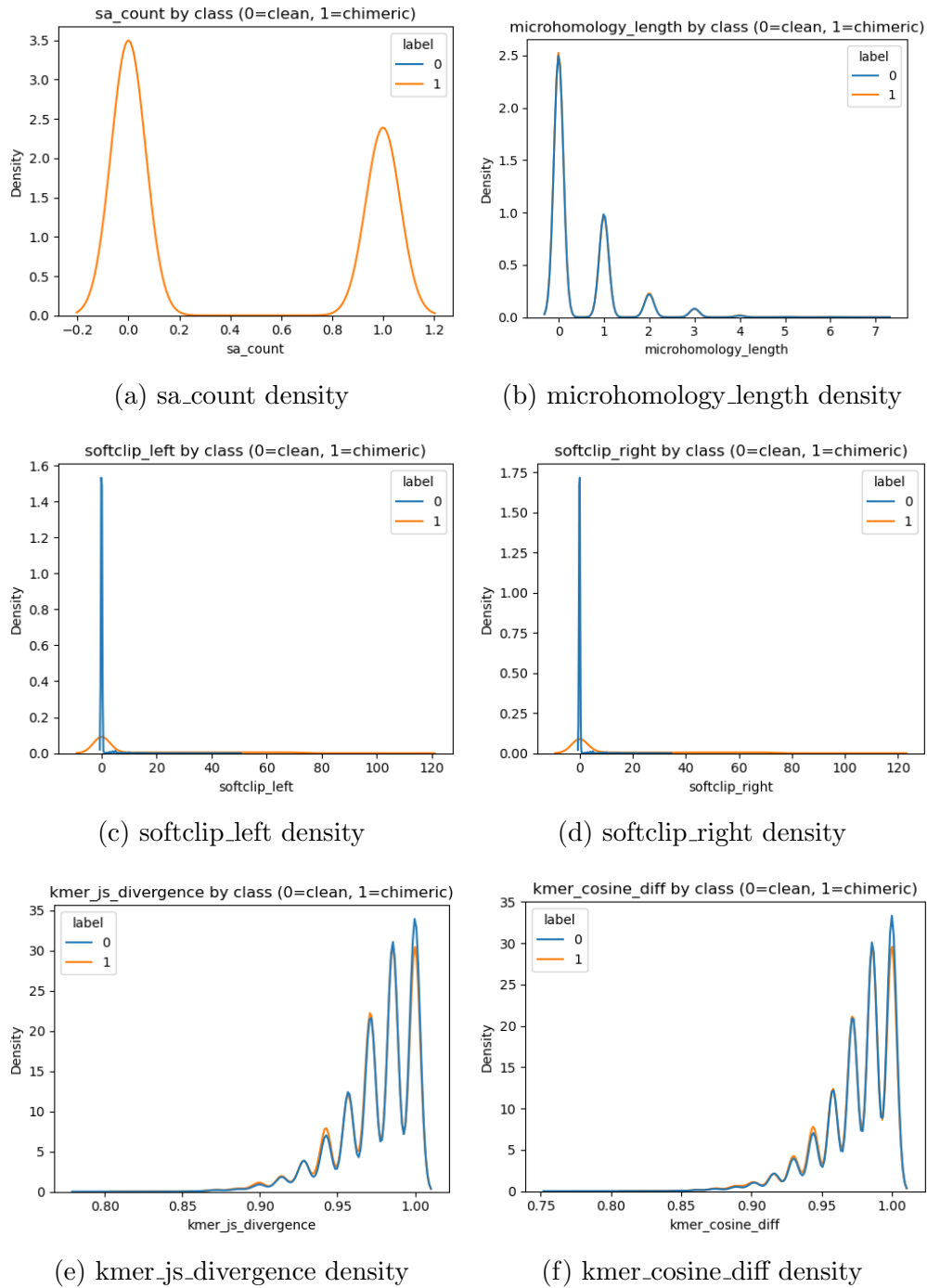


Figure 4.1: Kernel density plots of six key features comparing clean and chimeric reads.

750 4.2 Baseline Classification Performance

751 Table 4.1 summarises the performance of eleven classifiers trained on the engi-
752 neered feature set using five-fold cross-validation and evaluated on the held-out
753 test set. All models were optimised using default hyperparameters, without ded-
754 icated tuning.

755 The dummy baseline, which always predicts the same class regardless of the
756 input features, achieved an accuracy of 0.50 and test F1-score of 0.67. This re-
757 flects the balanced class distribution and provides a lower bound for meaningful
758 performance.

759 Across other models, test F1-scores clustered in a narrow band between ap-
760 proximately 0.74 and 0.77 and ROC–AUC values between 0.82 and 0.84. Gradi-
761 ent boosting, CatBoost, LightGBM, XGBoost, bagging trees, random forest, and
762 multilayer perceptron (MLP) all produced very similar scores, with CatBoost and
763 gradient boosting slightly ahead (test F1 \approx 0.77, ROC–AUC \approx 0.84). Linear
764 models (logistic regression and calibrated linear SVM) performed only marginally
765 worse (test F1 \approx 0.74), while Gaussian Naive Bayes lagged behind with substan-
766 tially lower F1 (\approx 0.65) despite very high precision for the chimeric class.

Table 4.1: Performance of baseline classifiers on the held-out test set.

model	test_accuracy	test_precision	test_recall	test_f1	test_roc_auc
dummy_baseline	0.500000	0.500000	1.000000	0.667000	0.500000
logreg_l2	0.789000	0.945000	0.614000	0.744000	0.821000
linear_svm_calibrated	0.789000	0.945000	0.614000	0.744000	0.820000
random_forest	0.788000	0.894000	0.654000	0.755000	0.834000
extra_trees	0.788000	0.901000	0.647000	0.753000	0.824000
gradient_boosting	0.802000	0.936000	0.648000	0.766000	0.840000
xgboost	0.800000	0.929000	0.650000	0.765000	0.839000
lightgbm	0.799000	0.926000	0.650000	0.764000	0.838000
catboost	0.803000	0.936000	0.650000	0.767000	0.839000
knn	0.782000	0.892000	0.642000	0.747000	0.815000
gaussian_nb	0.741000	0.996000	0.483000	0.651000	0.819000
bagging_trees	0.792000	0.900000	0.657000	0.760000	0.837000
mlp	0.789000	0.931000	0.625000	0.748000	0.819000

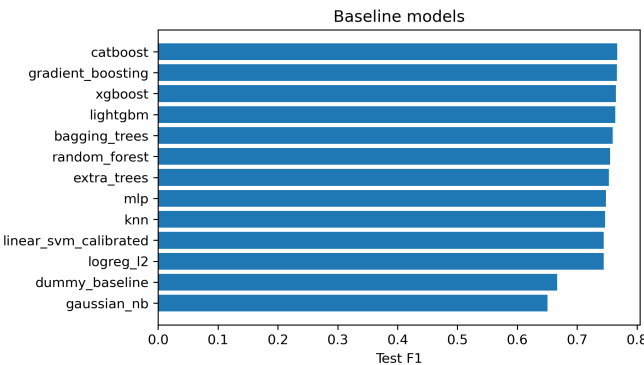


Figure 4.2: Test F1 of all baseline classifiers, showing that no single model clearly dominates and several achieve comparable performance.

767 4.3 Effect of Hyperparameter Tuning

768 To assess whether performance could be improved further, ten model families un-
 769 derwent randomised hyperparameter search (Chapter 3). The tuned metrics are
 770 summarised in Table 4.2. Overall, tuning yielded modest but consistent gains for
 771 tree-based ensembles and boosting methods, while leaving linear models essen-

772 tially unchanged or slightly worse.

773 CatBoost, gradient boosting, LightGBM, XGBoost, random forest, bagging
774 trees, and MLP all experienced small increases in test F1 (typically $\Delta F1 \approx 0.002 -$
775 0.009) and ROC–AUC (up to $\Delta AUC \approx 0.008$). After tuning, CatBoost remained
776 the best performer with test accuracy 0.802, precision 0.924, recall 0.658, F1-score
777 0.769, and ROC–AUC 0.844. Gradient boosting achieved almost identical perfor-
778 mance (F1 0.767, AUC 0.843). Random forest and bagging trees also improved
779 to F1 scores around 0.763 with AUC ≈ 0.842 .

Table 4.2: Performance of tuned classifiers on the held-out test set.

model	test_accuracy	test_precision	test_recall	test_f1	test_roc_auc
logreg_l2_tuned	0.788000	0.946000	0.612000	0.743000	0.818000
linear_svm_calibrated_tuned	0.788000	0.944000	0.612000	0.743000	0.818000
random_forest_tuned	0.797000	0.915000	0.655000	0.763000	0.842000
extra_trees_tuned	0.794000	0.910000	0.652000	0.760000	0.837000
gradient_boosting_tuned	0.802000	0.928000	0.654000	0.767000	0.843000
xgboost_tuned	0.799000	0.922000	0.653000	0.765000	0.839000
lightgbm_tuned	0.801000	0.930000	0.651000	0.766000	0.842000
catboost_tuned	0.802000	0.924000	0.658000	0.769000	0.844000
bagging_trees_tuned	0.798000	0.922000	0.650000	0.763000	0.842000
mlp_tuned	0.790000	0.934000	0.625000	0.749000	0.821000

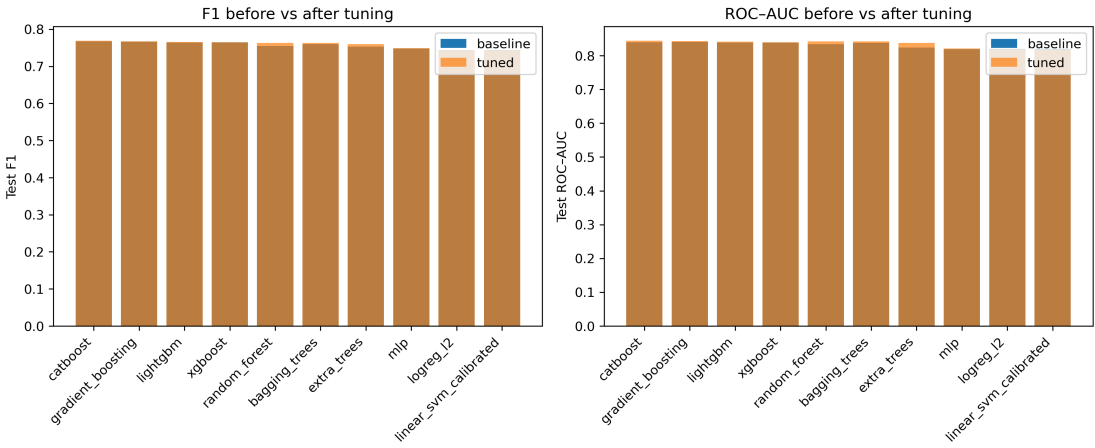


Figure 4.3: Comparison of test F1 (left) and ROC–AUC (right) for baseline and tuned models. Hyperparameter tuning yields small but consistent gains, particularly for tree-based ensembles.

780 Because improvements are small and within cross-validation variability, we
 781 interpret tuning as stabilising and slightly refining the models rather than funda-
 782 mentally altering their behaviour or their relative ranking.

783 4.4 Detailed Evaluation of Representative Mod- 784 els

785 For interpretability and diversity, four tuned models were selected for deeper
 786 analysis: CatBoost (best-performing boosted tree), scikit-learn gradient boost-
 787 ing (canonical gradient-boosting implementation), random forest (non-boosted
 788 ensemble baseline), and L2-regularised logistic regression (linear baseline). All
 789 models were trained on the engineered feature set and evaluated on the same
 790 held-out test data.

4.4.1 Confusion Matrices and Error Patterns

Classification reports and confusion matrices for the four models reveal consistent patterns. CatBoost and gradient boosting both reached overall accuracy of approximately 0.80 with similar macro-averaged F1 scores (~ 0.80). For CatBoost, precision and recall for clean reads were 0.73 and 0.95, respectively, while for chimeric reads they were 0.92 and 0.66 ($F1 = 0.77$). Gradient boosting showed nearly identical trade-offs.

Random forest attained slightly lower accuracy (0.80) and chimeric F1 (0.76), whereas logistic regression achieved the lowest accuracy among the four (0.79) and chimeric F1 (0.74), although it provided the highest chimeric precision (0.95) at the cost of lower recall (0.61).

Across all models, errors were asymmetric. False negatives (chimeric reads predicted as clean) were more frequent than false positives. For example, CatBoost misclassified 1 369 chimeric reads as clean but only 215 clean reads as chimeric. This pattern indicates that the models are conservative: they prioritise avoiding spurious chimera calls at the expense of missing some true chimeras. Depending on downstream application, alternative decision thresholds or cost-sensitive training could be explored to adjust this balance.

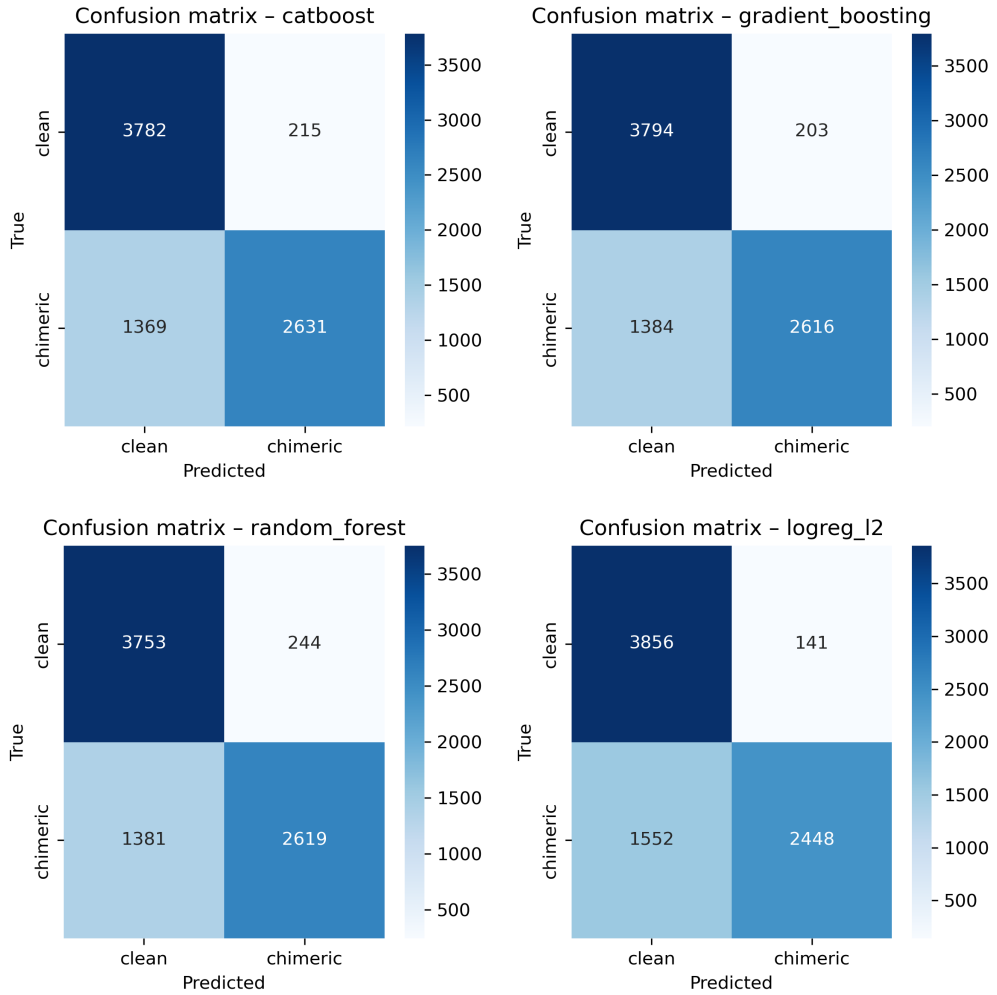


Figure 4.4: Confusion matrices for the four representative models on the held-out test set. All models show more false negatives (chimeric reads called clean) than false positives.

809 4.4.2 ROC and Precision–Recall Curves

810 Receiver operating characteristic (ROC) and precision–recall (PR) curves (Figure 4.5) further support the similarity among the top models. The three tree-based
 811 ensembles (CatBoost, gradient boosting, random forest) achieved ROC–AUC val-
 812 ues of approximately 0.84 and average precision (AP) around 0.88. Logistic re-
 813

814 gression performed slightly worse ($AUC \approx 0.82$, $AP \approx 0.87$) but still substantially
815 better than random guessing.

816 The PR curves show that precision remains above 0.9 across a broad range
817 of recall values (up to roughly 0.5–0.6), after which precision gradually declines.
818 This behaviour indicates that the models can assign very high confidence to a
819 subset of chimeric reads, while more ambiguous reads can only be recovered by
820 accepting lower precision.

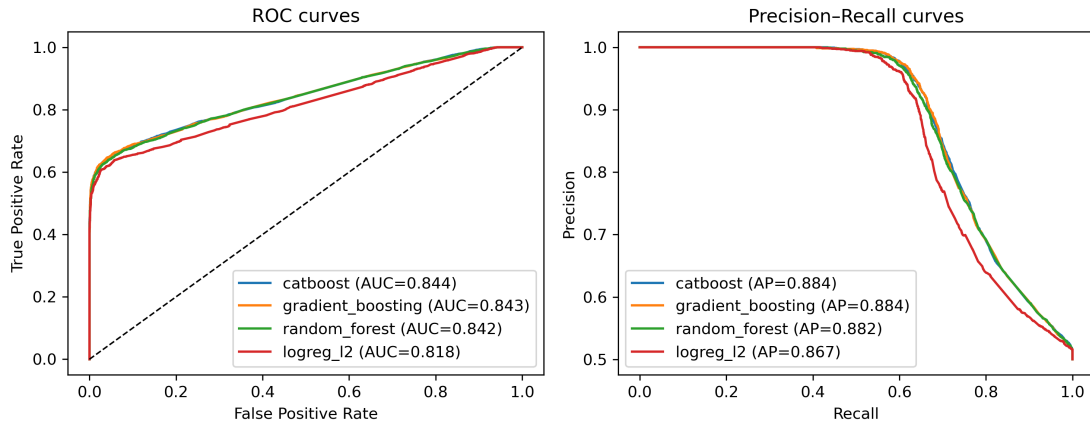


Figure 4.5: ROC (left) and precision–recall (right) curves for the four representative models on the held-out test set. Tree-based ensembles cluster closely, with logistic regression performing slightly but consistently worse.

821 References

- 822 Anderson, S., Bankier, A., Barrell, B., Bruijn, M., Coulson, A., Drouin, J., ...
823 Young, I. (1981, 04). Sequence and organization of the human mitochondrial
824 genome. *Nature*, *290*, 457-465. doi: 10.1038/290457a0
- 825 Arango, G., Garner, E., Pruden, A., Heath, L., Vikesland, P., & Zhang, L. (2018,
826 02). Deeparg: A deep learning approach for predicting antibiotic resistance
827 genes from metagenomic data. *Microbiome*, *6*. doi: 10.1186/s40168-018
828 -0401-z
- 829 Bentley, D. R., Balasubramanian, S., Swerdlow, H. P., Smith, G. P., Milton, J.,
830 Brown, C. G., ... Smith, A. J. (2008). Accurate whole human genome
831 sequencing using reversible terminator chemistry. *Nature*, *456*(7218), 53–
832 59. doi: 10.1038/nature07517
- 833 Boore, J. L. (1999). Animal mitochondrial genomes. *Nucleic Acids Research*,
834 *27*(8), 1767–1780. doi: 10.1093/nar/27.8.1767
- 835 Cameron, S. L. (2014). Insect mitochondrial genomics: Implications for evolution
836 and phylogeny. *Annual Review of Entomology*, *59*, 95–117. doi: 10.1146/
837 annurev-ento-011613-162007
- 838 Dierckxsens, N., Mardulyn, P., & Smits, G. (2017). Novoplasty: de novo assembly
839 of organelle genomes from whole genome data. *Nucleic Acids Research*,

- 840 45(4), e18. doi: 10.1093/nar/gkw955
- 841 Edgar, R. C. (2016). Uchime2: improved chimera prediction for amplicon se-
842 quencing. *bioRxiv*. Retrieved from <https://api.semanticscholar.org/>
843 CorpusID:88955007
- 844 Edgar, R. C. (n.d.). *Uchime in practice*. Retrieved from https://www.drive5.com/usearch/manual7/uchime_practical.html
- 845 Edgar, R. C., Haas, B. J., Clemente, J. C., Quince, C., & Knight, R. (2011).
846 Uchime improves sensitivity and speed of chimera detection. *Bioinformatics*,
847 27(16), 2194–2200. doi: 10.1093/bioinformatics/btr381
- 848 Glenn, T. C. (2011). Field guide to next-generation dna sequencers. *Molecular
849 Ecology Resources*, 11(5), 759–769. doi: 10.1111/j.1755-0998.2011.03024.x
- 850 Gonzalez, J. M., Zimmermann, J., & Saiz-Jimenez, C. (2004, 09). Evalu-
851 ating putative chimeric sequences from pcr-amplified products. *Bioin-
852 formatics*, 21(3), 333-337. Retrieved from <https://doi.org/10.1093/bioinformatics/bti008>
853 doi: 10.1093/bioinformatics/bti008
- 854 Gray, M. W. (2012). Mitochondrial evolution. *Cold Spring Harbor perspectives
855 in biology*, 4. Retrieved from <https://doi.org/10.1101/cshperspect.a011403>
856 doi: 10.1101/cshperspect.a011403
- 857 Hahn, C., Bachmann, L., & Chevreux, B. (2013). Reconstructing mitochondrial
858 genomes directly from genomic next-generation sequencing reads—a baiting
859 and iterative mapping approach. *Nucleic Acids Research*, 41(13), e129. doi:
860 10.1093/nar/gkt371
- 861 Jin, J.-J., Yu, W.-B., Yang, J., Song, Y., dePamphilis, C. W., Yi, T.-S., & Li,
862 D.-Z. (2020). Getorganelle: a fast and versatile toolkit for accurate de
863 novo assembly of organelle genomes. *Genome Biology*, 21(1), 241. doi:
864 10.1186/s13059-020-02154-5
- 865

- 866 Judo, M. S. B., Wedel, W. R., & Wilson, B. H. (1998). Stimulation and sup-
867 pression of pcr-mediated recombination. *Nucleic Acids Research*, *26*(7),
868 1819–1825. doi: 10.1093/nar/26.7.1819
- 869 Labrador, K., Agmata, A., Palermo, J. D., Ravago-Gotanco, R., & Pante, M. J.
870 (2021). Mitochondrial dna reveals genetically structured haplogroups of
871 bali sardinella (sardinella lemuru) in philippine waters. *Regional Studies in*
872 *Marine Science*, *41*, 101588. doi: 10.1016/j.rsma.2020.101588
- 873 Layer, R., Hall, I., & Quinlan, A. (2014, 10). Lumpy: A probabilistic framework
874 for structural variant discovery. *Genome Biology*, *15*. doi: 10.1186/gb-2014
875 -15-6-r84
- 876 Li, H. (2018, 05). Minimap2: pairwise alignment for nucleotide sequences. *Bioin-*
877 *formatics*, *34*(18), 3094-3100. Retrieved from <https://doi.org/10.1093/bioinformatics/bty191> doi: 10.1093/bioinformatics/bty191
- 879 Liang, Q., Bible, P. W., Liu, Y., Zou, B., & Wei, L. (2020, 02). Deepmi-
880 crobes: taxonomic classification for metagenomics with deep learning. *NAR*
881 *Genomics and Bioinformatics*, *2*(1), lqaa009. Retrieved from <https://doi.org/10.1093/nargab/lqaa009> doi: 10.1093/nargab/lqaa009
- 883 Metzker, M. L. (2010). Sequencing technologies — the next generation. *Nature*
884 *Reviews Genetics*, *11*(1), 31–46. doi: 10.1038/nrg2626
- 885 Mysara, M., Saeys, Y., Leys, N., Raes, J., & Monsieurs, P. (2015). Catch,
886 an ensemble classifier for chimera detection in 16s rrna sequencing stud-
887 ies. *Applied and Environmental Microbiology*, *81*(5), 1573-1584. Retrieved
888 from <https://journals.asm.org/doi/abs/10.1128/aem.02896-14> doi:
889 10.1128/AEM.02896-14
- 890 Peccoud, J., Lequime, S., Moltini-Conclois, I., Giraud, I., Lambrechts, L., &
891 Gilbert, C. (2018, 04). A survey of virus recombination uncovers canon-

- 892 ical features of artificial chimeras generated during deep sequencing li-
893 brary preparation. *G3 Genes—Genomes—Genetics*, 8(4), 1129-1138. Re-
894 trieved from <https://doi.org/10.1534/g3.117.300468> doi: 10.1534/
895 g3.117.300468
- 896 Qin, Y., Wu, L., Zhang, Q., Wen, C., Nostrand, J. D. V., Ning, D., ... Zhou, J.
897 (2023). Effects of error, chimera, bias, and gc content on the accuracy of
898 amplicon sequencing. *mSystems*, 8(6), e01025-23. Retrieved from <https://journals.asm.org/doi/abs/10.1128/msystems.01025-23> doi: 10.1128/
899 msystems.01025-23
- 900 Qiu, X., Wu, L., Huang, H., McDonel, P. E., Palumbo, A. V., Tiedje, J. M., &
901 Zhou, J. (2001). Evaluation of pcr-generated chimeras, mutations, and het-
902 eroduplexes with 16s rrna gene-based cloning. *Applied and Environmental
903 Microbiology*, 67(2), 880–887. doi: 10.1128/AEM.67.2.880-887.2001
- 904 Ren, J., Song, K., Deng, C., Ahlgren, N., Fuhrman, J., Li, Y., ... Sun, F. (2020,
905 01). Identifying viruses from metagenomic data using deep learning. *Quan-
906 titative Biology*, 8. doi: 10.1007/s40484-019-0187-4
- 907 Rodriguez-Martin, B., Palumbo, E., Marco-Sola, S., Griebel, T., Ribeca, P.,
908 Alonso, G., ... Djebali, S. (2017, 01). Chimpipe: Accurate detection of
909 fusion genes and transcription-induced chimeras from rna-seq data. *BMC
910 Genomics*, 18. doi: 10.1186/s12864-016-3404-9
- 911 Rognes, T., Flouri, T., Nichols, B., Quince, C., & Mahé, F. (2016). Vsearch: a
912 versatile open source tool for metagenomics. *PeerJ*, 4, e2584. doi: 10.7717/
913 peerj.2584
- 914 Sedlazeck, F., Rescheneder, P., Smolka, M., Fang, H., Nattestad, M., von Haeseler,
915 A., & Schatz, M. (2018, 06). Accurate detection of complex structural
916 variations using single-molecule sequencing. *Nature Methods*, 15. doi: 10
917

- 918 .1038/s41592-018-0001-7
- 919 Sfeir, A., & Symington, L. S. (2015). Microhomology-mediated end joining: A
920 back-up survival mechanism or dedicated pathway? *Trends in Biochemical
921 Sciences*, 40(11), 701-714. Retrieved from <https://www.sciencedirect.com/science/article/pii/S0968000415001589> doi: <https://doi.org/10.1016/j.tibs.2015.08.006>
- 923
- 924 Vervier, K., Mahé, P., Tournoud, M., Veyrieras, J.-B., & Vert, J.-P. (2015,
925 11). Large-scale machine learning for metagenomics sequence classifica-
926 tion. *Bioinformatics*, 32(7), 1023-1032. Retrieved from <https://doi.org/10.1093/bioinformatics/btv683> doi: 10.1093/bioinformatics/btv683
- 927
- 928 Willette, D., Bognot, E., Mutia, M. T., & Santos, M. (2011). *Biology and ecology
929 of sardines in the philippines: A review* (Vol. 13; Tech. Rep. No. 1). NFRDI
930 Technical Paper Series. Retrieved from <https://nfrdi.da.gov.ph/tpjf/etc/Willette%20et%20al.%20Sardines%20Review.pdf>
- 931